

Bottomonium precision tests from full lattice QCD: hyperfine splitting, Υ leptonic width and b quark contribution to $e^+e^- \rightarrow \text{hadrons}$.

D. Hatton^{*} and C. T. H. Davies[†]

SUPA, School of Physics and Astronomy, University of Glasgow, Glasgow, G12 8QQ, UK

J. Koponen

Helmholtz Institute Mainz, Johannes Gutenberg-Universität Mainz, 55099 Mainz, Germany

G. P. Lepage

Laboratory for Elementary-Particle Physics, Cornell University, Ithaca, New York 14853, USA

A. T. Lytle

Department of Physics. University of Illinois, Urbana, IL 61801, USA

(HPQCD collaboration)[‡]

(Dated: November 29, 2021)

We calculate the mass difference between the Υ and η_b and the Υ leptonic width from lattice QCD using the Highly Improved Staggered Quark formalism for the b quark and including u , d , s and c quarks in the sea. We have results for lattices with lattice spacing as low as 0.03 fm and multiple heavy quark masses, enabling us to map out the heavy quark mass dependence and determine values at the b quark mass. Our results are: $M_\Upsilon - M_{\eta_b} = 57.5(2.3)(1.0)$ MeV (where the second uncertainty comes from neglect of quark-line disconnected correlation functions) and decay constants, $f_{\eta_b} = 724(12)$ MeV and $f_\Upsilon = 677.2(9.7)$ MeV, giving $\Gamma(\Upsilon \rightarrow e^+e^-) = 1.292(37)(3)$ keV. The hyperfine splitting and leptonic width are both in good agreement with experiment, and provide the most accurate lattice QCD results to date for these quantities by some margin. At the same time results for the time moments of the vector-vector correlation function can be compared to values for the b quark contribution to $\sigma(e^+e^- \rightarrow \text{hadrons})$ determined from experiment. Moments 4–10 provide a 2% test of QCD and yield a b quark contribution to the anomalous magnetic moment of the muon of $0.300(15) \times 10^{-10}$. Our results, covering a range of heavy quark masses, may also be useful to constrain QCD-like composite theories for beyond the Standard Model physics.

I. INTRODUCTION

Weak decay matrix elements calculated in lattice QCD are critical to the flavour physics programme of over-determining the Cabibbo-Kobayashi-Maskawa (CKM) matrix to find signs of new physics. For that programme the weak decays of b quarks are particularly important since they give access to the least well known CKM elements, V_{ub} and V_{cb} . These CKM matrix elements can be determined either using exclusive decay channels and lattice QCD form factors or inclusive decay channels and measured spectral shape functions. There continues to be some tension between the exclusive and inclusive determinations [1] that needs further improvements to both approaches to resolve. On the lattice QCD side this means developing improved approaches to B meson weak decay matrix elements, such as [2, 3], but also providing more stringent tests of lattice QCD results in b physics to make sure that sources of systematic error are under full control. Here we provide three such tests using bottomonium correlation functions; the ground-state hyperfine splitting (the mass difference between the Υ and

η_b), the Υ leptonic width and the b quark contribution to $R(e^+e^- \rightarrow \text{hadrons})$. The latter two, being electromagnetic processes, can be compared with experiment free from CKM uncertainties. We obtain the most accurate results to date for these quantities and are able to include the effect of the b quark's electric charge in the calculation for the first time.

We use the Highly Improved Staggered Quark (HISQ) discretisation of the quark action for these calculations. The HISQ action was developed in [4] to have small discretisation errors with the leading errors, quadratic in the lattice spacing, removed. This makes the action particularly good for heavier quarks when discretisation errors appear as powers of the quark mass in lattice units, which can be relatively large. This action enabled the first accurate lattice calculations in charm physics [5–8]. More recently it has been used to achieve sub-1% accuracy in the charmonium hyperfine splitting, J/ψ leptonic width, m_c and c quark vacuum polarisation contribution to the anomalous magnetic moment of the muon [9]. The calculation used a range of lattice spacing values from 0.15 fm to 0.03 fm with u , d , s and c quarks in the sea and included the effect of the c quark's electric charge [9].

Here we will extend this latter calculation to bottomonium. Because the b quark mass is much larger than that of c , we need fine lattices to reach the b with a quark mass in lattice units, $am_b < 1$ and controlled discreti-

^{*} daniel.hatton@glasgow.ac.uk

[†] christine.davies@glasgow.ac.uk

[‡] <http://www.physics.gla.ac.uk/HPQCD>

sation errors. Our strategy, known as the heavy-HISQ approach [10], is to perform calculations for a range of masses between c and b on lattices with a range of fine lattice spacings. We can then map out the dependence on the heavy quark mass both of the quantity being calculated and its discretisation errors. This enables us to determine a physical result at the b quark mass.

This approach has been very successful for decay constants and spectroscopy for heavy-light (B , B_s and B_c) mesons [10–12] and is now being used for the form factors for B meson weak decays [2, 3]. Here we will apply this approach to the Υ for the first time.

There are alternative nonrelativistic approaches that can be used at the b quark mass on coarser lattices; see [13] for the determination of the Υ and Υ' leptonic widths using lattice NonRelativistic QCD. The nonrelativistic expansion of the Hamiltonian and the currents that appear in matrix elements gives systematic uncertainties from missing higher-order relativistic corrections and from renormalisation of the lattice current to match the continuum current. These uncertainties hinder tests at high precision.

In contrast the HISQ action is relativistic and the HISQ vector current can be matched accurately and fully nonperturbatively to that in continuum QCD [14]. As we will show below, this enables us to improve the lattice QCD accuracy on the bottomonium hyperfine splitting to better than 5% and to achieve percent-level precision on the Υ and η_b decay constants and on moments that parameterise the b quark contribution to $R(e^+e^- \rightarrow \text{hadrons})$.

Our results cover the range of heavy quark masses from c to b and we will give results for decay constant to mass ratios over this range. These could be useful both for tuning of phenomenological models of QCD but also as constraints on QCD-like composite theories for beyond the Standard Model physics.

The paper is organised as follows. In the next Section we give details of the lattice calculation we perform. This includes a general description of the fits that we use to determine the heavy mass dependence of the quantities calculated. We then present results for the bottomonium hyperfine splitting in Section III, the decay constants for both the η_b and Υ in Section IV and the time-moments of the vector current-current correlators in Section V. Each section includes a description of the calculation and then a discussion subsection with comparison to experiment and previous lattice QCD results. Section IV on decay constants also includes plots of decay constant to mass ratios and the ratio of vector to pseudoscalar decay constants over the quark mass range from c to b . We then give our conclusions in Section VI.

II. LATTICE CALCULATION

We use ensembles of lattice gluon field configurations provided by the MILC collaboration [15] at values of

the lattice spacing, $a \approx 0.09$ fm, 0.06 fm, 0.045 fm and 0.03 fm. The configurations are generated with an $\alpha_s a^2$ -improved discretisation of the gluon action [16] and include the effect of u , d , s and c quarks in the sea with the HISQ formalism [4]. The u and d masses are taken to be the same and we denote this mass m_l . For most of the ensembles we have unphysically heavy u/d quarks with $m_l/m_s \approx 0.2$ but we employ two ensembles with physical values of m_l and lattice spacing values 0.09 fm and 0.06 fm. We expect sea quark mass effects to be small for the Υ because it has no valence light quarks. However, an analysis of such effects is needed for accurate results.

Table I lists the parameters of the ensembles that we use. The lattice spacing is determined in terms of the Wilson flow parameter w_0 [17]. On these ensembles we calculate quark propagators from random wall sources using the HISQ action and with a variety of masses, m_h , from that of the c quark upwards. The valence heavy quark masses that we use on each ensemble are listed in Table II. The value of ϵ_{Naik} used in the coefficient of the Naik term in the HISQ action [4] is taken as the tree-level function of the quark mass given in [6].

We combine the quark propagators into (connected) meson correlation functions for both pseudoscalar (η_h) and vector (ϕ_h) mesons, using the local γ_5 and γ_i operators converted to appropriate form for staggered quarks [8, 9]. Note that we do not include quark-line disconnected correlation functions that take account of the heavy quark/antiquark annihilation to gluons. We expect the effect of the disconnected correlation functions to be very small in the heavyonium system. In [9] our result for the mass difference between J/ψ and η_c mesons was accurate enough, for the first time, to see a difference with experiment of 7.3(1.2) MeV. We concluded that this was the effect of the missing disconnected correlation function on the η_c mass. Here we will test for a similar effect on the η_b .

On the coarsest two ensembles we use 16 time-sources on each gluon field configuration for high statistics; we take 8 time-sources on the other ensembles. We use at least 100 configurations on each ensemble for a good statistical sample. In generating the very fine lattice (set 6 in Table I) a slow evolution in Monte Carlo time of the topological charge was observed [15], so that the ensemble does not explore many topological sectors. However, it has been shown that the impact of this on calculations for heavy mesons is negligible [18].

We fit the correlation functions from each ensemble using a multi-exponential constrained fit [21] and following the method in [9]. The fit form used for the pseudoscalar correlators as a function of t , the time separation between source and sink, is

$$C_P(t) = \sum_i A_i^P f(E_i^P, t), \quad (1)$$

and the vector fit form is

$$C_V(t) = \sum_i \left(A_i^V f(E_i^V, t) - (-1)^t A_i^{V,o} f(E_i^{V,o}, t) \right). \quad (2)$$

TABLE I. Sets of MILC configurations [15] used here with HISQ sea quark masses, m_l^{sea} ($l = u/d$), m_s^{sea} and m_c^{sea} given in lattice units. The lattice spacing is given in units of w_0 [17]; the physical value of w_0 was determined to be 0.1715(9) fm from f_π [19]. Sets 1 and 2 are ‘fine’ ($a \approx 0.09$ fm), sets 3 and 4 are ‘superfine’ ($a \approx 0.06$ fm), set 5 ‘ultrafine’ ($a \approx 0.045$ fm) and set 6 ‘exafine’ ($a \approx 0.03$ fm). The final two columns give the extent of the lattice in each spatial direction (L_s) and time (L_t).

Set	label	w_0/a	am_l^{sea}	am_s^{sea}	am_c^{sea}	L_s	L_t
1	f-5	1.9006(20)	0.0074	0.037	0.440	32	96
2	f-phys	1.9518(7)	0.00120	0.0363	0.432	64	96
3	sf-5	2.8960(60)	0.00480	0.0240	0.286	48	144
4	sf-phys	3.0170(23)	0.0008	0.022	0.260	96	192
5	uf-5	3.892(12)	0.00316	0.0158	0.188	64	192
6	ef-5	5.243(16)	0.00223	0.01115	0.1316	96	288

Here

$$f(E, t) = e^{-Et} + e^{-E(L_t - t)}. \quad (3)$$

The term that oscillates in time in the vector case results from the use of staggered quarks. E_0 is the mass of the lowest lying state (either pseudoscalar or vector) and A_0 is related to the meson decay constants. The ground-state pseudoscalar meson we will denote as η_h and the vector as ϕ_h . We fit the correlation functions for all masses on a given ensemble simultaneously (with two exceptions, see Table II). This means that the correlations between results for different masses are carried through the rest of the calculation. The correlations between the ϕ_h and η_h correlators are safely neglected as the uncertainty in the ϕ_h results dominates that for the η_h . Results for the ground-state mesons are listed in Table II.

We also have a limited amount of data which includes the effects of quenched QED (electrically charged valence quarks, but not sea quarks). This allows us to assess the impact of QED and appropriately account for it in our error budgets. As in [9] we use photon fields in Feynman gauge in the QED_L formalism [22]. Our quenched QED calculations [9, 20] used a valence quark electric charge of $2/3e$ (i.e. the charge on a c quark), where e is the magnitude of the charge on an electron. We can use these results to determine the electromagnetic correction for the b electric charge of $-(1/3)e$. Given the smallness of α_{QED} we take QED corrections to be linear in the quark charge squared, Q^2 , and simply rescale the effect of QED by a factor of $1/4$ from that for $Q = (2/3)e$. Results are given in Table III in the form of the ratio, R^0 , of results in QCD+QED to those in pure QCD at a fixed value of the valence quark mass in lattice units. We see there that the impact of QED is tiny but visible. We showed in [9] that QED finite-volume effects were negligible for the electrically neutral charmonium mesons. This will continue to be true for the heavier mesons that we study here and so we ignore such effects.

As we showed in [9], fixing the lattice spacing from w_0

and f_π , as we have done, means that QED corrections to the lattice spacing should be at the sub-0.1% level (coming from QED effects in the quark sea). We can therefore compare QCD plus quenched QED to pure QCD using the same value of the lattice spacing (i.e. that from Table I). QED affects the tuning of the lattice quark masses, however. We use the simple and natural scheme of tuning the b quark mass in both the QCD+QED and pure QCD cases so that the Υ mass has the physical value. We can then use our results to determine the impact of QED on the quantities we study, taking the renormalisation of the quark mass into account. We will give that information, after fitting, as the renormalised ratio R which is the ratio of the QCD+QED result to that in pure QCD when both theories have a b quark mass separately tuned so that the Υ mass takes the experimental value in both cases.

For each quantity that we study we must fit our results, in physical units, as a function of heavy quark mass and lattice spacing to determine results in the continuum limit at the physical b quark mass. We will use the ϕ_h mass as a physical proxy for the heavy quark mass and then the physical point is defined by the ϕ_h mass becoming equal to that of the Υ .

In previous studies of heavy meson masses and decay constants using the heavy-HISQ method the HPQCD collaboration have used fit forms that capture the heavy mass dependence as a polynomial in the inverse H_s or η_h mass [10, 11]. In the case of heavy-light mesons this form is justified by the heavy quark effective theory (HQET) expansion. In the case of heavyonium the HQET expansion is not valid but the same form may still be expected to work as a Taylor expansion over a finite region in m_h . Here, however, we choose to use a fit form that is more agnostic with regards to the dependence on the heavy quark mass. We achieve this by using cubic splines between specified knot positions¹. We do not expect to need many knots because the quantities we study here should be smooth monotonic functions of M_{ϕ_h} in the continuum limit at physical sea quark masses. The fit function for our lattice results also needs to include dependence on the lattice spacing and the mistuning of sea quark masses. Both of these effects can also depend on the heavy quark mass (M_{ϕ_h}) through smooth monotonic functions and so we also include cubic splines in their description.

We use fits of the following form for the pure QCD

¹ We use splines that are monotonic between knots (Steffen splines [23]).

TABLE II. Results in lattice units for the masses of the ground-state pseudoscalar meson, η_h , and ground-state vector meson, ϕ_h , for valence heavy quark masses in lattice units listed in column 2, for the ensembles listed in column 1. Results come from simultaneous fits to all heavy quark masses on a given ensemble, except for the cases marked with an asterisk [20]. These used different random numbers for the sources and so are not correlated with the other results for that ensemble. Column 5 gives the mass difference in lattice units between the ϕ_h and η_h , column 6 the η_h decay constant and column 7 the raw (unrenormalised) ϕ_h decay constant. The required Z_V factors are taken from [14].

Set	am_h	aM_{η_h}	aM_{ϕ_h}	$a\Delta M_{\text{hyp}}$	af_{η_h}	af_{ϕ_h}/Z_V
1	0.6	1.675554(47)	1.717437(70)	0.041882(84)	0.208641(60)	0.21865(11)
	0.8	2.064088(40)	2.101542(57)	0.037454(70)	0.249695(64)	0.25711(10)
2	0.6	1.674264(13)	1.715453(32)	0.041189(35)	0.207535(22)	0.21690(10)
	0.8	2.063015(11)	2.099940(26)	0.036925(29)	0.248493(21)	0.255249(96)
	0.866*	2.185464(53)	2.221789(38)	0.036325(65)	0.264483(61)	0.27011(12)
3	0.274	0.896664(33)	0.929876(86)	0.033212(92)	0.117554(37)	0.12339(15)
	0.4	1.175559(29)	1.202336(85)	0.026778(90)	0.135692(39)	0.13916(21)
	0.5	1.387459(27)	1.411113(72)	0.023654(77)	0.148936(40)	0.15104(20)
	0.548*	1.487111(36)	1.509697(54)	0.022586(65)	0.155563(68)	0.157200(87)
	0.6	1.593089(25)	1.614626(63)	0.021537(68)	0.162314(41)	0.16318(19)
	0.7	1.793118(23)	1.813249(57)	0.020131(61)	0.176638(42)	0.17617(19)
	0.8	1.987504(22)	2.006783(52)	0.019279(56)	0.192680(44)	0.19061(19)
4	0.260	0.862671(27)	0.895702(52)	0.033030(58)	0.114147(34)	0.11969(10)
	0.4	1.173904(23)	1.199806(36)	0.025903(43)	0.134475(37)	0.137266(83)
	0.6	1.591669(19)	1.612586(27)	0.020917(34)	0.161035(39)	0.161236(77)
	0.8	1.986246(17)	2.005047(24)	0.018801(29)	0.191297(41)	0.188634(82)
5	0.194	0.666821(41)	0.692026(59)	0.025205(72)	0.087774(42)	0.091442(91)
	0.4	1.130722(31)	1.147617(40)	0.016895(51)	0.114953(46)	0.114918(72)
	0.6	1.549098(26)	1.562884(32)	0.013786(41)	0.137487(54)	0.135412(69)
	0.8	1.945787(23)	1.958252(27)	0.012465(35)	0.162850(58)	0.158238(72)
	0.9	2.135642(21)	2.147903(25)	0.012261(33)	0.178229(58)	0.171745(74)
6	0.138	0.496969(42)	0.516149(61)	0.019180(74)	0.065916(59)	0.06841(10)
	0.45	1.201328(29)	1.211601(28)	0.010273(40)	0.102989(81)	0.100572(70)
	0.55	1.410659(27)	1.420048(24)	0.009389(36)	0.112668(82)	0.109506(67)
	0.65	1.614877(24)	1.623684(21)	0.008807(32)	0.122639(81)	0.118680(64)

TABLE III. Quenched QED corrections, for quark electric charge $e/3$, to a subset of the results of Table II presented as the ratio, R^0 , of the value in QCD+QED to that in pure QCD at fixed valence quark mass in lattice units.

Set	am_h	$R_{\text{QED}}^0[aM_{\eta_h}]$	$R_{\text{QED}}^0[aM_{\phi_h}]$	$R_{\text{QED}}^0[a\Delta M_{\text{hyp}}]$	$R_{\text{QED}}^0[af_{\eta_h}]$	$R_{\text{QED}}^0[af_{\phi_h}/Z_V]$
2	0.866	1.0002170(45)	1.0002637(14)	1.00307(25)	1.001255(68)	1.001343(62)
3	0.274	1.0003937(42)	1.0004468(28)	1.001875(83)	1.00078(12)	1.000708(83)
	0.548	1.0003306(12)	1.00036876(24)	1.002882(80)	1.001127(35)	1.0009805(75)

part of our fit:

$$\begin{aligned}
F(a, M_{\phi_h})[\text{QCD}] = & A[F_0(M_{\phi_h}) + G_0(1/M_{\phi_h})] \quad (4) \\
& + \sum_{i=1}^3 G_1^{(i)}(M_{\phi_h})(am_h)^{2i} \\
& + \sum_{j=1}^3 G_2^{(j)}(M_{\phi_h})(a\Lambda)^{2j} \\
& + G_3(M_{\phi_h})(a\Lambda)^2(am_h)^2 \\
& + \sum_{k=0}^2 G_4^{(k)}(M_{\phi_h})(am_h)^{2k}\delta_l \\
& + G_5(M_{\phi_h})\delta_c]
\end{aligned}$$

$F(a, M_{\phi_h})$ are the lattice QCD results in physical units of GeV for the hyperfine splitting and decay constants

and GeV^{-1} for the time-moments. A is then a dimensionful number of a size commensurate with the size of the quantity being fitted (this will be given in each section) so that the rest of the fit in square brackets is dimensionless. F_0 is a dimensionless function of M_{ϕ_h} that differs between the different quantities we examine (and will also be given in each section). It is a very simple function of M_{ϕ_h} that captures the general trend in the mass dependence, on top of which the corrections modelled by splines are relatively minor. G_n denotes a cubic spline. All of the splines have different parameters but keep the same positions for the knots. The splines are functions of M_{ϕ_h} , where M_{ϕ_h} is in GeV, except for the first spline, G_0 , which provides the physical corrections to F_0 . We found that a spline in $1/M_{\phi_h}$ rather than M_{ϕ_h} gave a better χ^2 for quantities like the hyperfine splitting which fall as M_{ϕ_h} grows, approximately as the inverse.

We allow for two kinds of discretisation effects, those that are set by the heavy quark mass am_h and those that are independent of the heavy quark mass and instead are set by a fixed scale that we call Λ . We take Λ to be 0.5 GeV. The $G_1^{(i)}$ splines allow for heavy mass dependence in the am_h discretisation effects and the $G_2^{(j)}$ splines allow for heavy mass dependence in the $a\Lambda$ discretisation effects. We also include a mixed term in $(am_h)^2(a\Lambda)^2$ with spline G_3 , although this has little impact on the fits.

The last two lines of the fit form in Eq. (4) allow for sea quark mass mistunings. The light quark mass mistuning parameter δ_l is defined as:

$$\delta_l = \frac{2m_l^{\text{sea}} + m_s^{\text{sea}} - 2m_l^{\text{phys}} - m_s^{\text{phys}}}{10m_s^{\text{phys}}}. \quad (5)$$

m_s^{phys} and m_l^{phys} are taken to be the same as those used in [9]. The charm quark mass mistuning parameter is defined similarly:

$$\delta_c = \frac{m_c^{\text{sea}} - m_c^{\text{phys}}}{10m_c^{\text{phys}}}. \quad (6)$$

We allow for discretisation effects and heavy mass dependence set by splines $G_4^{(k)}$ within the light sea quark mistuning term. We allow for heavy mass dependence in the sea charm mass mistuning term through the spline G_5 .

For data that includes quenched QED effects we add extra terms to the fit function in Eq. (4). The full fit takes the form:

$$F(a, M_{\phi_h})[\text{QCD} + \text{QED}] = F(a, M_{\phi_h})[\text{QCD}] + A\alpha_{\text{QED}}Q^2 \left[\hat{G}_1(1/M_{\phi_h}) + c_{\text{QED}, am_h} \hat{G}_2(M_{\phi_h})(am_h)^2 \right]. \quad (7)$$

\hat{G}_1 and \hat{G}_2 are additional spline functions.

For all the fits considered here we use knots placed at $\{2.5, 4.9, 10\}$ GeV, taking knots at the beginning and end of the fit range and one in the middle. This is the optimal number of knots according to the Bayes Factor. We have checked that varying the sums over discretisation effects so that the number of terms included changes by ± 1 has no significant effect. Because statistical errors are so small here (see Table II) we employ an SVD (singular value decomposition) cut [24] in the fit to account for tiny effects that are too small to be modelled by our fit form of Eq. 4. The SVD cut value times the maximum eigenvalue of the covariance matrix sets a minimum value for the eigenvalues. Any eigenvalues of the covariance matrix below this minimum are then replaced with the minimum value. This is a conservative move which increases our uncertainties, as can be seen from the impact of the SVD cut in our error budgets.

The prior information given to the fit are central values and widths for the values of the coefficients, c_F , in F_0 and for the values of the spline functions at each knot. We use priors of 0 ± 1 for all of these. We use the `lsqfit` python

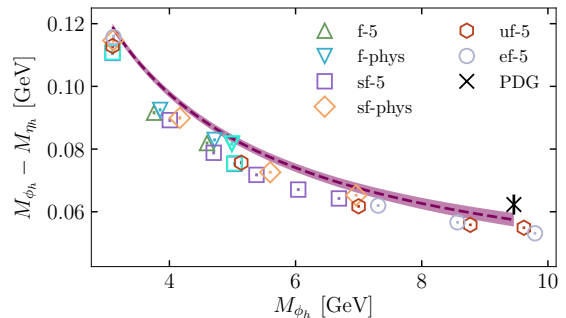


FIG. 1. The heavyonium hyperfine splitting as a function of the vector heavyonium mass, M_{ϕ_h} . The points show our lattice results from Tables II and III, with different symbols denoting different ensembles as in the legend. The errors are dominated by uncertainties from a that are correlated between the points. QCD+QED points are shown in cyan. They are not distinguishable from their pure QCD counterparts, but are visible by being shown on top of these values. Cubic splines are used to fit the heavy mass dependence, as described in the text. The fit evaluated at the physical point and zero lattice spacing is given by purple dashed line with error band. The experimental average value for the hyperfine splitting [1] is plotted as the black cross at the physical Υ mass.

module [25] to do the fits, implementing the splines with the `gvar` module [26].

To obtain our final results, the fit function is evaluated at lattice spacing equal to zero, sea quark masses tuned to their physical values and M_{ϕ_h} equal to M_Υ . This is taken from experiment as 9.4603 GeV [1] with negligible uncertainty.

III. HYPERFINE SPLITTING

The hyperfine splitting, ΔM_{hyp} , is the difference in mass between the ground-state ϕ_h and η_h mesons. The values for the hyperfine splitting on each ensemble for a variety of heavy quark masses are given in column 5 of Table II. The separate η_h and ϕ_h masses are given in lattice units in columns 3 and 4. The impact of quenched QED at fixed valence quark mass is given in Table III. The effect of QED is similar to that for charmonium [9] but reduced because of the smaller electric charge of the b quark. The direct effect of QED on the hyperfine splitting is to increase it, through a QED hyperfine effect which has the same sign as the QCD hyperfine effect. QED also increases the meson masses, however, and this requires a retuning of the bare quark masses downwards to match the same meson mass. This then has an indirect effect, increasing the hyperfine splitting by a very small amount.

Our lattice results are plotted in Fig 1 as a function of the vector heavyonium mass, M_{ϕ_h} . The points include both pure QCD and QCD+QED values but the

QCD+QED values are indistinguishable from pure QCD on this scale.

To fit our results for the hyperfine splitting using Eq. (4) we take $A = 0.1$ GeV and the simple form for F_0 , $F_0 = c_F^{(0)} + c_F^{(1)}(3 \text{ GeV})/M_{\phi_h}$. The coefficients $c_F^{(0)}$ and $c_F^{(1)}$ have prior values 0(1). Note that we multiply the QED correction term in the fit (Eq. (7)) by a factor of 2 because of the size of the QED corrections that we see in the results (Table III and [20]). That these prior widths are very conservative can be judged from the values and variation across Fig. 1. Evaluating the fit result at zero lattice spacing, tuned quark masses and with M_{ϕ_h} equal to the Υ mass, we obtain the physical result for the bottomonium hyperfine splitting using connected correlation functions of:

$$M_\Upsilon - M_{\eta_b} (\text{connected}) = 57.5(2.3) \text{ MeV}. \quad (8)$$

This is the QCD+QED value. For the ratio of the QCD+QED value to the pure QCD result, we obtain:

$$R_{\text{QED}}[\Delta M_{\text{hyp}}] = 1.0001(26). \quad (9)$$

Note that this is the ‘renormalised’ ratio with the b quark mass tuned from the Υ in both QCD+QED and QCD. We see no significant impact of quenched QED at the 0.2% level. The fit has a χ^2/dof of 0.73 using an SVD cut of 5×10^{-3} .

Fig. 1 shows our fit curve as a function of M_{ϕ_h} in the continuum limit for tuned sea quark masses. This gives useful physical insight into how the hyperfine splitting falls as the quark mass increases. At the high mass end of the plot we mark with a black cross the experimental average value [1] for the bottomonium system. We will discuss the comparison to experiment further in Section III A. We note that at the lower mass end of the curve we have results for charmonium. Our fit here does not include all of the charmonium results that went into [9] but gives a value for the charmonium hyperfine splitting that is consistent (within 1σ) with [9] for the pure QCD case. The QED+QCD result here is too small at the charmonium end of the fit curve because the QED is being included with quark charge $1/3e$ rather than the correct charm quark charge of $2/3e$.

We will discuss in Section III A what the impact of quark-line disconnected (but gluon-connected) correlation functions could be on the bottomonium hyperfine splitting. For our charmonium calculation of [9] we included an estimate of the QED quark-line disconnected contribution to the hyperfine splitting coming from $c\bar{c}$ annihilation to a single photon, which then converts back to $c\bar{c}$. The contribution of this to the charmonium hyperfine splitting is 0.7 MeV, which was a little more than half the uncertainty in our result. The equivalent contribution for the Υ here is much smaller, at 0.17 MeV, because of the smaller electric charge of the b quark. At a size of one tenth of the uncertainty in our result in Eq. (8), this would then have negligible impact and we do not include it.

TABLE IV. Error budget for the hyperfine splitting and decay constants as a percentage of the final answer.

	$M_\Upsilon - M_{\eta_b}$	f_Υ	f_{η_b}
statistics	2.40	0.77	0.38
SVD cut	1.48	0.44	0.67
w_0	0.55	0.61	0.59
w_0/a	0.66	0.23	0.18
Z_V	-	0.29	-
F_0	0.03	0.01	0.00
G_0	0.05	0.02	0.01
G_1	1.14	0.17	0.18
G_2	0.48	0.24	0.31
G_3	0.42	0.28	0.45
G_4	1.45	0.73	0.98
G_5	1.08	0.29	0.27
\hat{G}_1	0.29	0.07	0.08
\hat{G}_2	0.19	0.01	0.00
Total (%)	3.99	1.43	1.59

A complete error budget for the bottomonium hyperfine splitting is given in Table IV. Statistical uncertainties are divided between those arising from our 2-point fits and those coming from the lattice spacing determination, both correlated between ensembles (w_0) and uncorrelated (w_0/a). The uncertainty from the 2-point fits is further divided in two. As already mentioned, the use of an SVD cut is conservative and increases the uncertainty in the fit output. We can calculate the contribution to an error budget of both the data with and without the SVD cut applied to its correlation matrix. In the error budgets of Table IV we give the contribution from the data with the original correlation matrix under the heading ‘statistics’. The additional contribution from the SVD cut is then defined as the square root of the difference of the squared contributions from the data with and without an SVD cut applied. The contributions from various parts of the heavy mass dependence in Eqs. (4) and (7) are shown individually, labelled by the set of spline functions for that contribution.

The fit parameters required to reproduce the physical curve of the hyperfine splitting as a function of M_{ϕ_h} plotted in Fig. 1 are given in Table IX of Appendix A.

A. Discussion: Hyperfine splitting

Our bottomonium hyperfine splitting result of Eq. 8 is compared to earlier lattice QCD results in Fig. 2, going back to the first lattice QCD calculation to include sea quarks [27]. Clearly the use of the heavy-HISQ approach has allowed us to reduce the uncertainty significantly (by a factor of 3) relative to these earlier results. The earlier results all use non-relativistic actions, or actions with non-relativistic input such as the Fermilab formalism [36], for the b quarks. This leads to uncertainties from the normalisation of relativistic corrections to the Hamiltonian, such as the $\sigma \cdot B$ term that is responsible

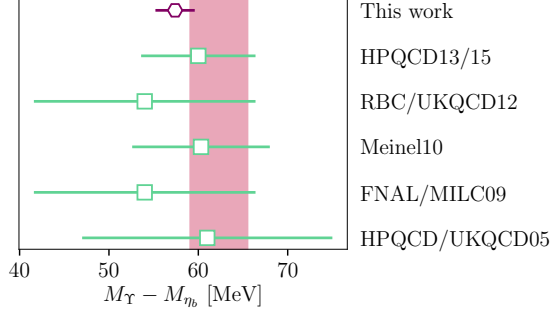


FIG. 2. Comparison of lattice QCD determinations of the bottomonium hyperfine splitting. Our result from Eq. (8) is given by the top purple hexagon. Previous results (green squares) come from: HPQCD/UKQCD using $\mathcal{O}(v^4)$ NRQCD b quarks and 2+1 flavours of asqtad sea quarks [27]; the Fermilab Lattice/MILC collaborations using the Fermilab formalism for the b quark and 2+1 flavours of asqtad sea quarks [28]; S.Meinel using NRQCD b quarks with $\mathcal{O}(v^6)$ spin-dependent terms and 2+1 flavours of domain-wall sea quarks [29]; the RBC/UKQCD collaboration using the RHQ formalism for the b quark and 2+1 flavours of domain-wall sea quarks [30] and HPQCD using radiatively-improved NRQCD b quarks with $\mathcal{O}(v^6)$ spin-dependent terms and 2+1+1 flavours of HISQ sea quarks [31]. All of these results come from calculation of connected correlation functions and do not include an uncertainty from missing quark-line disconnected diagrams, except for [31]. [31] includes the effect of these disconnected diagrams through the inclusion of 4-quark operators with coefficients, calculated in perturbation theory through $\mathcal{O}(\alpha_s)$. See the text for discussion of the impact on the hyperfine splitting through η_b annihilation to gluons. The red band is the PDG experimental average [1]. The result for the hyperfine splitting calculated here shows a clear improvement on previous lattice QCD results, as well as being the first to include QED effects. This improvement is in large part due to the elimination of systematic uncertainties from the use of nonrelativistic actions which arise in previous calculations.

for the hyperfine splitting. We avoid this uncertainty with the HISQ action at the cost of having to calculate at multiple heavy quark masses rather than directly at the b quark mass.

As discussed in Sec. II, we have only computed connected correlators. This is also true for the earlier results except for that in [31]. This means that we are neglecting the contribution to the η_b mass from its annihilation to gluons. This contribution can be related to the η_b hadronic width using NRQCD perturbation theory [4]:

$$\Delta M_{\eta_b} = \frac{\Gamma_{\eta_b}}{2} \left(\frac{2(\ln 2 - 1)}{\pi} + \mathcal{O}(\alpha_s, v^2/c^2) \right). \quad (10)$$

Using the total width of the η_b of 10(5) MeV [1] gives a shift to the η_b mass from the leading order term of -1.0(5) MeV. This would result in an upward shift in the hyperfine splitting of approximately 1 MeV, which amounts to 0.5σ for our result (Eq. (8)).

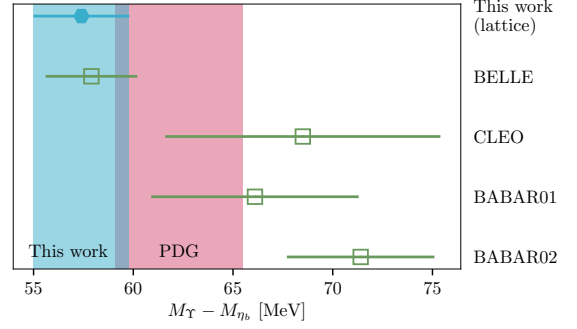


FIG. 3. Comparison of different experimental results for the bottomonium hyperfine splitting. The red band shows the PDG average of these experimental results [1]. The filled blue hexagon is our result (Eq. (11)) and is carried downwards as the blue band. Note that our result here includes an uncertainty from the effect of η_b annihilation missing from our lattice calculation. There is some tension between the different experimental results with our value favouring the most recent result from BELLE [32]. The result labelled CLEO is from [33], BABAR01 from [34] and BABAR02 from [35].

We recently showed, for the first time, that this leading-order analysis fails in the case of the charmonium hyperfine splitting [9] where, with the improved accuracy we were able to achieve, it becomes clear that the lattice QCD+QED result is significantly higher than the experimental average. Assuming that this difference is the result of the effect of η_c annihilation missing from the lattice calculation, it seems that the leading-order perturbative analysis is misleading in this case. Presumably missing higher-order terms in the perturbative analysis or nonperturbative effects from mixing between the η_c and other flavour-singlet pseudoscalar mesons [37], or both combined, have a larger effect than the leading-order term and opposite sign. In the bottomonium case the η_b is considerably further from these lighter states and so we may expect a much smaller effect from this. We also expect perturbation theory to be more reliable at the higher energy associated with bottomonium states.

We therefore allow an additional 1 MeV uncertainty for the impact of η_b annihilation on the hyperfine splitting and give a final result of

$$M_{\Upsilon} - M_{\eta_b} = 57.5(2.3)(1.0) \text{ MeV}. \quad (11)$$

The first uncertainty is from the lattice calculation and the second from missing quark-line disconnected contributions.

The experimental average value for the bottomonium hyperfine splitting (62.3 ± 3.2 MeV) [1] is shown by a red band on Fig. 2. A more detailed comparison with experimental results is given in Fig. 3. This makes clear the spread in the experimental results, handled in [1] by increasing the uncertainty in the average by a factor of 1.8. In particular it shows that the most recent and most precise result from BELLE [32] is noticeably lower than

the others. This BELLE result is in agreement with our determination to within 1σ .

Our result is also in agreement with the PDG average to within 1.5σ . We see no disagreement with the experimental result that would signal a larger contribution from η_b annihilation than the 1 MeV that we have allowed above. Indeed a shift upwards of our hyperfine splitting result by 1 MeV, as suggested by leading-order perturbation theory, would improve the agreement between lattice QCD and experiment, although the shift would not be significant. In contrast, a shift downwards of the bottomonium hyperfine splitting by several MeV, as we found for the charmonium hyperfine splitting, would cause tension with the experimental results.

Finally we note that the high precision we are able to achieve for the bottomonium hyperfine splitting is the result of concentrating on the ground-state mesons with a highly-improved relativistic action. For a more complete picture of the bottomonium spectrum, obtained on an anisotropic lattice with the Fermilab heavy quark action and focussing on highly excited states see [38].

IV. Υ AND η_b DECAY CONSTANTS

We define the vector heavyonium meson (ϕ_h) decay constant from the annihilation matrix element as

$$\langle 0 | \bar{\psi} \gamma^i \psi | \phi_h \rangle = f_{\phi_h} M_{\phi_h} \epsilon^i. \quad (12)$$

This means that we can determine the decay constant from our fits to the vector meson correlation functions using:

$$\frac{af_{\phi_h}}{Z_V} = \sqrt{\frac{2A_0^V}{E_0^V}}, \quad (13)$$

where A_0^V is the ground-state amplitude from a correlator fit of the form given in Eq. (2). Z_V is the renormalisation constant required to match the local vector current in lattice QCD to that of continuum QCD at each value of the lattice spacing. We use Z_V values calculated in a nonperturbative implementation of the RI-SMOM scheme [14, 39, 40]. The pure QCD results for Z_V for the HISQ action are given in [9, 14]; we use values at scale $\mu = 2$ GeV. Note that no additional matching factor is required to reach $\overline{\text{MS}}$ from the RI-SMOM scheme and, because Z_V has no anomalous dimensions, any μ dependence is purely a discretisation effect [14].

The vector meson decay constant is the amplitude for annihilation of the valence quark/antiquark pair, into a photon, for example. It is related to the experimentally measurable leptonic width by:

$$\Gamma(\phi_h \rightarrow e^+ e^-) = \frac{4\pi}{3} \alpha_{\text{QED}}^2 e_h^2 \frac{f_{\phi_h}^2}{M_{\phi_h}} \quad (14)$$

where e_h is the quark electric charge (1/3 for b). The α_{QED} here is evaluated at the mass of the heavy quark and is equal to 1/132.15 [41] at the b .

We also compute the decay constant of the pseudoscalar heavyonium meson, f_{η_h} . In terms of the parameters of our correlator fit, Eq. (1) this is defined as:

$$f_{\eta_h} = 2m_h \sqrt{\frac{2A_0^P}{(E_0^P)^3}}. \quad (15)$$

Because the partially conserved axial current (PCAC) relation holds for HISQ quarks the pseudoscalar decay constant is absolutely normalised and no Z factor is required to match to the continuum regularisation of QCD. Since the pseudoscalar meson does not annihilate to a single particle, there is no experimental decay process that gives direct access to the decay constant. Its value is nevertheless of interest for comparison to that of the corresponding vector meson and other pseudoscalar mesons.

The values of the decay constants, in lattice units, on each ensemble and for each heavy mass are given in the sixth and seventh columns of Table II. The decay constants converted to GeV units, and renormalised in the case of the vector decay constant, are plotted as a function of the ϕ_h mass in Fig. 4. The decay constants increase with increasing ϕ_h mass. Discretisation effects are clearly visible that cause the lattice results to peel away from the physical curve upwards. The same effect was seen previously for both heavy-light and heavyonium mesons [10, 11].

We also show results in Fig. 4 that include the effect of quenched QED. Those results are given in Table III as the ratio of values in QCD+QED to those in pure QCD. For the decay constant of the ϕ_h these ratios do not include the impact of QED on the vector current renormalisation factor, Z_V . This was calculated in [14] for the case of a quark with electric charge $2e/3$, again as a ratio of results in QCD+QED to those in pure QCD. These results are given in Table IV of [14], with further results in Table X of [9]. The ratio is within 0.05% of 1, as expected for an $\mathcal{O}(\alpha_{\text{QED}})$ correction to a Z factor that is already very close to 1 for the HISQ action in pure QCD. Here we need results for an electric charge of $e/3$ so we determine the ratios in QCD+QED to pure QCD in that case by taking the values from [9, 14] (for $\mu = 2$ GeV) and dividing the difference from 1 by a factor of four.

To fit our decay constant results as a function of lattice spacing and heavy quark mass we again use the fit form of Eq. (4) but we use $A = 0.7$ GeV, as appropriate for the decay constant values, and a different form for F_0 to that used for the hyperfine splitting case. The dependence of the decay constants on the heavy mass is approximately linear and so we choose $F_0 = c_F^{(0)} + c_F^{(1)} M_{\phi_h} / (3 \text{ GeV})$, where $c_F^{(0)}$ and $c_F^{(1)}$ are fit parameters with prior values of 0 ± 1 . We fit the ϕ_h and η_h decay constants simultaneously, including the correlations between them and take the same F_0 for both since they are so close in value. The spline functions that map out the differences from F_0 in physical heavy quark mass dependence and the dependence on the lattice spacing and sea quark masses take independent values in the two cases. The fit has a

χ^2/dof value of 0.44 using an SVD cut of 1×10^{-4} . We again evaluate our fits at zero lattice spacing, physical sea quark masses and with $M_{\phi_h} = M_{\Upsilon}$ to obtain the physical bottomonium results.

We obtain, for the Υ ,

$$f_{\Upsilon} = 677.2(9.7) \text{ MeV} \quad (16)$$

with

$$R_{\text{QED}}[f_{\Upsilon}] = 1.00004(76). \quad (17)$$

For the η_b ,

$$f_{\eta_b} = 724(12) \text{ MeV}, \quad (18)$$

with

$$R_{\text{QED}}[f_{\eta_b}] = 1.00017(71). \quad (19)$$

Again, QED effects are not discernible within our 0.1% uncertainties. At the charmonium end of our range our results agree within uncertainties with the values we obtained in [9], remembering that the calculation done here is for an electric charge that does not match that of the c quark. The error budget for both decay constants is given in Table IV. The fit curves evaluated at zero lattice spacing and physical sea quark masses are plotted as a function of heavy quark mass (given by M_{ϕ_h}) in Fig. 4. The fit parameters required to reproduce these physical curves of the decay constants as a function of M_{ϕ_h} are given in Table X of Appendix A.

Given that the heavy mass dependence and discretisation effects in the vector and pseudoscalar decay constants are similar we can study the ratio of the two as a function of the heavy mass to high precision. Our results for the ratio are shown as a function of M_{ϕ_h} in Fig. 5. A slow downward drift of the ratio is seen with increasing M_{ϕ_h} from a value slightly above 1 for c quarks to a value slightly below 1 for b quarks.

To obtain a physical result for the ratio we again use the fit form of Eq. (4), now taking F_0 to be a constant, c_F , since the ratio is relatively flat, so that the spline functions handle all of the mass dependence. We take the prior value of c_F to be 1(1), i.e. with a very conservative width. Since we expect a lot of systematic effects to cancel in this ratio (and Fig. 5 shows that they do) we halve the prior widths on all of the correction terms in Eq. 4 i.e. we take prior values on the function values at the knots of 0.0(5). The fit has a χ^2/dof of 0.22 and no SVD cut is required. Evaluating the fit function at the physical point gives

$$\frac{f_{\Upsilon}}{f_{\eta_b}} = 0.9454(99), \quad (20)$$

and

$$R_{\text{QED}} \left[\frac{f_{\Upsilon}}{f_{\eta_b}} \right] = 0.99994(38). \quad (21)$$

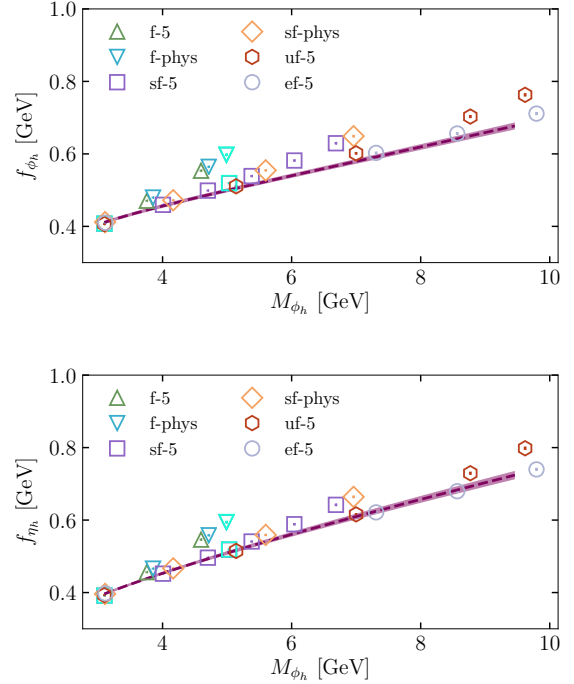


FIG. 4. Upper panel: The ϕ_h decay constant plotted against the ϕ_h mass. The symbols correspond to different gluon field ensembles, as given in the legend (see Table I for a list). Points including quenched QED are shown in cyan, indistinguishable from pure QCD points underneath. The dashed line and error band show the fit described in the text evaluated at zero lattice spacing and physical sea quark masses. Lower panel: The η_h decay constant plotted against the ϕ_h mass, symbols and fit line as above.

The total uncertainty in the ratio for the b is 1%, with a value clearly below 1. The fit curve evaluated at zero lattice spacing and physical sea quark masses is plotted as a function of M_{ϕ_h} in Fig. 5. The fit parameters required to reproduce this physical curve are given in Table XI of Appendix A.

A. Discussion : Decay constants

Figure 6 compares our result for the Υ decay constant, f_{Υ} , to that of an earlier lattice QCD calculation on a subset of the same gluon field configurations used here but using an improved NRQCD action for the b quarks [13]. Clearly, we achieve a considerably improved uncertainty over that of [13]. A large amount of the NRQCD uncertainty arises from the normalisation and $\mathcal{O}(v^2/c^2)$ improvement of the NRQCD vector current, where v is the nonrelativistic quark velocity. Here, since we use the HISQ action which is relativistic and we have performed the vector current renormalisation to very high precision previously [14], these sources of uncertainty are effectively eliminated.

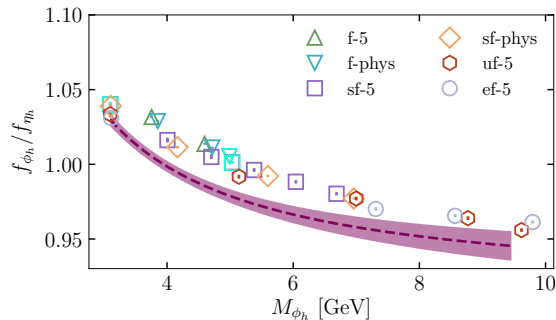


FIG. 5. The ratio of the vector to pseudoscalar heavyonium decay constants as a function of vector heavyonium mass. At the charmonium point the ratio is above 1. By the bottomonium point the ratio has shifted to be below 1. The symbols correspond to results on the different gluon field configurations listed in the legend with cyan points corresponding to QCD+QED. The line is the fit curve evaluated at the physical point as a function of M_{ϕ_h} described in the text.

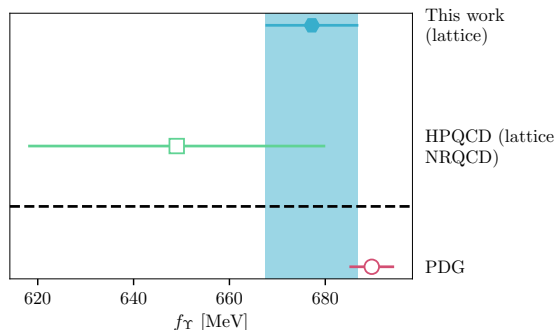


FIG. 6. A comparison of our result (filled blue hexagon) for the decay constant of the Υ with HPQCD's earlier lattice QCD result using NRQCD b quarks [13] (open green square). We also include the value inferred from the experimental leptonic decay width in Eq. (22) (pink open circle).

Figure 6 also compares our result for f_{Υ} to that obtained from the experimental average for the Υ leptonic width using Eq. (14). Using $\Gamma(\Upsilon \rightarrow e^+e^-) = 1.340(18)$ keV [1] gives

$$f_{\Upsilon}^{\text{expt}} = 689.7(4.6)(0.8) \text{ MeV} \quad (22)$$

where the first uncertainty comes from the experimental uncertainty in Γ and the second allows for an $\mathcal{O}(\alpha_{\text{QED}}/\pi)$ uncertainty from higher-order in QED terms in Eq. (14) coming, for example, from final-state radiation. Note that using α_{QED} of 1/137 here instead of 1/132.15 would increase the experimental value of f_{Υ} by 3.7% or 25 MeV. This is several times larger than either the experimental uncertainty or our lattice QCD uncertainty.

Figure 6 shows good agreement, within 1σ , between our lattice QCD result and that from experiment (eq. (22)). The experimental uncertainty is about half

that from our lattice QCD result.

Our result for f_{Υ} can be converted into a determination of the width for Υ decay to light leptons in the Standard Model using Eq. (14). This gives

$$\Gamma(\Upsilon \rightarrow e^+e^-) = 1.292(37)(3) \text{ keV} \quad (23)$$

where the first uncertainty comes from the lattice QCD result and the second allows for a relative $\mathcal{O}(\alpha_{\text{QED}}/\pi)$ correction to Eq. (14) from higher-order QED effects.

Our result for f_{η_b} can be compared to an earlier HPQCD lattice QCD result using HISQ quarks and the heavy-HISQ approach on gluon field configurations including the effect of 2+1 flavours of asqtad sea quarks [11]. That work obtained a value $f_{\eta_b} = 667(6)$ MeV, which is significantly lower (by 4σ) than our result here. The discrepancy is most likely to result from a bias in the earlier results from not having values on lattices with spacings as fine as we do here. Another possible source of the discrepancy is the fact that the earlier calculation did not include c quarks in the sea. Having more flavours of quarks in the sea results in a slower running of the strong coupling constant. Hence, using the language of potential models, we expect the Coulomb-like term in the heavy quark potential (of the form $-4\alpha_s(r)/(3r)$) to have a larger value for α_s at the short-distance scales to which the η_b meson decay constant is sensitive. This corresponds to a deeper potential at short distances and a correspondingly larger ‘wavefunction-at-the-origin’, which is the quantity in a potential model that translates approximately into the decay constant. This effect could explain some of the discrepancy but is unlikely to be large enough to explain it all. The calculations in [11] also used a different form to fit the lattice results as a function of heavy quark mass (in that case using as proxy M_{η_h}). This consisted of multiple powers of the inverse heavy quark mass multiplied by a leading function of the form $(M/M_0)^b$ where b was allowed to float. We have checked that using that fit form here gives us results for f_{η_b} very consistent with our spline fits, so the discrepancy with [11] is not related to the form of the fit used.

The ratio of vector to pseudoscalar decay constants as a function of heavyonium mass provides a test of our understanding of these mesons. In the language of potential models the heavyonium vector and pseudoscalar mesons differ only through spin-dependent relativistic corrections to the central potential [42]. The size of relativistic corrections fall as the heavy quark mass increases and the mean squared-velocity of the heavy quarks fall. In the infinite quark mass limit pseudoscalar and vector heavyonium mesons have the same mass and the same wavefunction-at-the-origin. The decay constants differ, however, by the matching factors that are needed to renormalise temporal axial and spatial vector currents from this nonrelativistic framework to full continuum QCD. The ratio of the vector to pseudoscalar heavyonium decay constants would then be expected to become the ratio of the vector to temporal axial vector matching

factors in the heavy quark limit. The matching factors come from high-momentum regions of phase-space and so can be calculated in QCD perturbation theory. An $\mathcal{O}(\alpha_s)$ matching calculation was done in [43] for spin-independent nonrelativistic QCD and gave the result

$$\frac{Z_V}{Z_A} = 1 - \frac{g^2}{6\pi^2} = 1 - \frac{2\alpha_s}{3\pi}. \quad (24)$$

From this we conclude that we would expect the ratio of vector to pseudoscalar decay constants to be below 1 for large heavy quark mass. Eq. (24) expects the difference from 1 to be $\mathcal{O}(5\%)$, taking $\alpha_s \approx 0.25$, but this formula will have corrections from higher orders in α_s . A value for the ratio of 5% below 1 is very consistent with our results in Fig. 5, however.

Very similar behaviour is seen for the ratio of vector to pseudoscalar decay constants for heavy-light mesons from lattice QCD calculations. The decay constant of the D_s^* meson is found to be several percent larger than that of the D_s [44–46] whereas that of the B_s^* is a few percent below that of the B_s [47] [45]. This behaviour can be understood on the same basis as the arguments for heavyonium above. In the heavy-light case an α_s^3 calculation of the matching factors is available in the infinite heavy quark mass limit [48]. The corrections to the $\mathcal{O}(\alpha_s)$ formula for the ratio (which is the same as for heavyonium in Eq. (24)) are sizeable but have the same (negative) sign and so do not change the qualitative behaviour of the difference of the ratio from 1.

Having performed the fits of the previous subsections we now have physical values for the decay constants not only at the b quark mass but at the full range of masses between the c and b quark masses. The physical curves as a function of meson mass in Figs. 4 and 5 could be used to tune phenomenological QCD potential models, that often differ markedly on features of heavyonium physics such as details of the wavefunction even when reproducing the spectrum (see, for example [50–52]).

They may also be useful beyond QCD. In [49] lattice QCD results across a range of masses were collected with the intention of providing useful information for phenomenologists studying strongly coupled beyond the Standard Model (BSM) theories. These theories are often QCD-like but typically with heavier (relative to the confinement scale) fundamental fermions than the light quarks of QCD. Ref. [49] makes the point that information from lattice QCD calculations about how (for example) meson masses and decay constants depend on quark masses can be useful to constrain such BSM theories. This then requires lattice QCD results for quark masses not at their physical values, as we have here. The lattice QCD results need to be presented in an appropriate way with dimensionless combinations of decay constants and masses on both axes. A convenient x -axis is the ratio of pseudoscalar to vector meson mass. In [49] the square of this quantity was used since the lattice QCD results were concentrated at light quark masses. Here, since we have heavy quarks and the ratio of pseudoscalar to vector

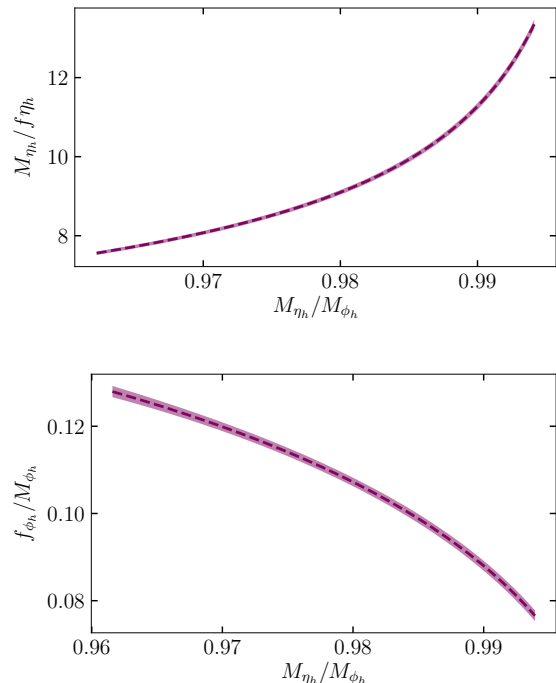


FIG. 7. Upper plot: The physical ratio (evaluated at zero lattice spacing and with sea quark mass mistunings set to zero) of the mass to decay constant for the pseudoscalar heavyonium meson, η_h as a function of the ratio of pseudoscalar to vector heavyonium masses. Lower plot: The physical ratio of decay constant to mass for the vector heavyonium meson, ϕ_h , (the quantity denoted f_V in [49]) plotted against the same ratio of masses.

meson masses is close to 1, we simply use the ratio.

Dimensionless ratios are readily obtained for our raw lattice results using the values in Table II. Correlations can be ignored because statistical uncertainties are so small. In the following we construct appropriate ratios from our fit functions in the limit of zero lattice spacing and physical sea quark masses and do not include the raw lattice results in the figures, for clarity.

One useful quantity [53] is the ratio of the pseudoscalar meson mass and decay constant for a meson made of quarks of degenerate mass (i.e. the ‘pions’ of the BSM model). Using the physical heavy mass dependence of f_{η_h} extracted from our fit we display the ratio of M_{η_h} and f_{η_h} as a function of the ratio of pseudoscalar to vector meson masses in Fig. 7. Our results show values of M_{η_h}/f_{η_h} around 10, and continuing to rise, as the ratio of pseudoscalar to vector meson masses heads towards 1. Note that our definition of the pseudoscalar decay constant in Eq. (15) corresponds to the normalisation $f_\pi \approx 130$ MeV.

As discussed in [49] composite models of a dark sector in which a ‘dark ρ ’ meson couples to ordinary matter through a dark photon (e.g. [54]) need information on the vector meson decay constant for an appropriate

range of fermion masses. The ratio of vector meson decay constant to vector meson mass is denoted f_V in [49]. In our convention for the vector meson decay constant (Eq. (12)) it is f_{ϕ_h}/M_{ϕ_h} . We plot f_{ϕ_h}/M_{ϕ_h} against the pseudoscalar to vector meson mass ratio in Fig. 7. We see that this ratio becomes small as the ratio of pseudoscalar to vector meson masses heads towards 1. It also has relatively strong dependence on the mass ratio, so using an approximately constant value (based, for example, on naive dimensional analysis) would not agree well with our results.

We also note that accurate lattice QCD results are available at the ratio of pseudoscalar to vector meson masses of 0.673 which corresponds to $s\bar{s}$ mesons when only connected correlation functions are calculated. This means that the pseudoscalar meson is not allowed to annihilate and mix with flavour-singlet mesons made from lighter quarks, and likewise the vector decay to two pseudoscalar mesons incorporating lighter quarks is not included. This is then the scenario that would match that required in a composite BSM scenario. For this case HPQCD calculates $M_{\eta_s}/f_{\eta_s} = 3.801(16)$ [19] and $f_{\phi_s}/M_{\phi_s} = 0.233(3)$ [55]. These results must connect smoothly to the ones shown in Fig. 7 as the quark mass is increased.

V. VECTOR CURRENT-CURRENT CORRELATOR TIME-MOMENTS AND a_μ^b

The ground-state vector heavyonium decay constant is determined by the amplitude of the state that dominates the correlator at large times and this can be connected to experiment via the leptonic width, as we have seen. We can also calculate the time moments of the correlator. These depend on the behaviour of the correlator at shorter time distances and can also be connected to experimental results [8, 56]. The moments of the vector heavyonium correlator are defined by:

$$G_n^V = Z_V^2 \sum_{\tilde{t}} \tilde{t}^n C_{\phi_h}(\tilde{t}) \quad (25)$$

where \tilde{t} is lattice time symmetrised around the centre of the lattice, C_{ϕ_h} is the vector two-point correlation function and Z_V is the renormalisation factor for the heavyonium vector current operator used.

Results for $(G_n^V/Z_V^2)^{1/(n-2)}$ in lattice units on each of our ensembles are given in Table V for $n = 4$ to 10. The power $1/(n-2)$ is taken to reduce all the moments to the same dimension. We take the Z_V factor for the vector current to be the same one used for the leptonic width above [14]. Figure 8 then shows the physical results for these moments as a function of M_{ϕ_h} .

Results that include quenched QED corrections for a subset of ensembles are given in Table VI. These are given as the ratio of the result in QCD+QED to that in QCD at fixed valence quark mass in lattice units. The values of R^0 are very slightly below 1, as for charmonium [9].

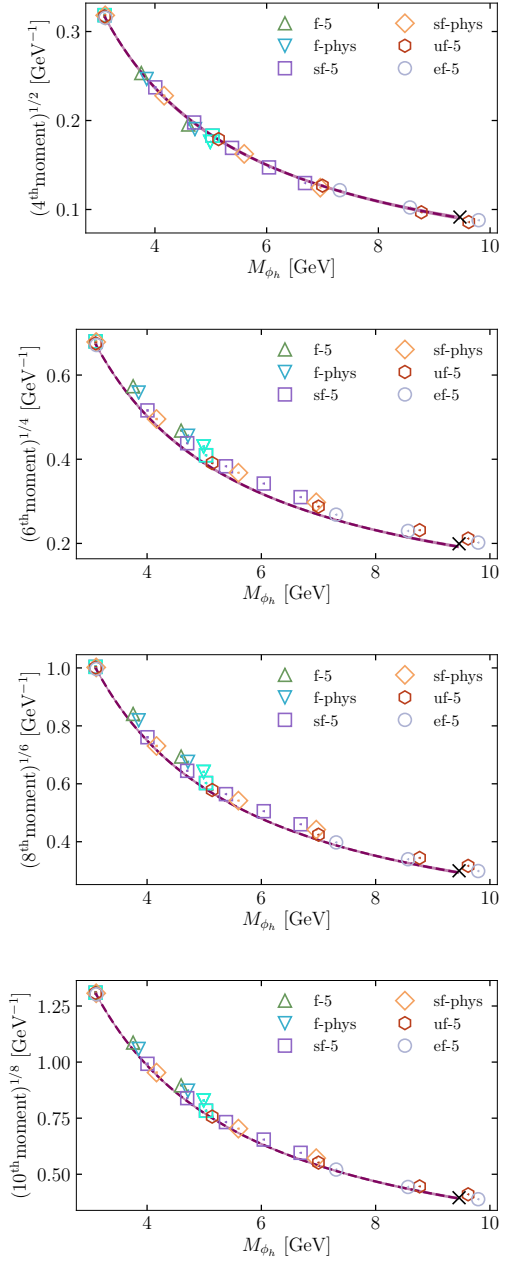


FIG. 8. Results for the 4th, 6th, 8th and 10th time moments of the heavyonium vector correlator plotted as a function of M_{ϕ_h} . The symbols correspond to different gluon field ensembles, as given in the legend (see Table I for a list). The errors on the points are dominated by uncertainties from the determination of Z_V that are correlated between the points. Points including quenched QED are shown in cyan, indistinguishable from pure QCD points underneath. The dashed line with purple error band displays our continuum/chiral fit, as discussed in the text. Values determined from experimental results for $R_{e^+e^-}$ (eq. (26)) are plotted as the black crosses at $M_{\phi_h} = M_\gamma$ [57].

The difference from 1 is even smaller here because of the smaller quark electric charge. Note that the vector

TABLE V. Results in lattice units for time moments of the vector heavyonium correlator as defined in Eq. (25). We give raw results here in which the vector current has not been renormalised and we also take the $(n-2)$ th root to reduce all the moments to the same dimensions. The numbers in the table are then $(G_n^V/Z_V^2)^{1/(n-2)}$ for $n=4$ to 10.

Set	am_h	$n=4$	$n=6$	$n=8$	$n=10$
1	0.6	0.562768(11)	1.263877(18)	1.849015(25)	2.386587(33)
	0.8	0.4342507(59)	1.0316257(96)	1.525578(12)	1.967383(15)
2	0.6	0.5628101(56)	1.2640282(83)	1.849341(10)	2.387158(12)
	0.8	0.4342571(32)	1.0316599(48)	1.5256620(57)	1.9675445(65)
	0.866	0.395358(44)	0.966054(54)	1.439945(54)	1.861205(52)
3	0.274	1.070712(58)	2.27651(10)	3.35545(14)	4.37419(17)
	0.4	0.797940(92)	1.72744(16)	2.54252(21)	3.31432(25)
	0.5	0.665034(57)	1.466318(96)	2.15508(13)	2.80305(16)
	0.548	0.60993(22)	1.36481(25)	2.00869(24)	2.61113(24)
	0.6	0.569093(37)	1.282926(63)	1.886184(84)	2.44653(10)
	0.7	0.495371(26)	1.145651(43)	1.689190(58)	2.186270(72)
	0.8	0.436182(18)	1.037685(31)	1.538234(41)	1.989299(51)
	0.866	0.395358(44)	0.966054(54)	1.439945(54)	1.861205(52)
4	0.260	1.114660(44)	2.366266(78)	3.48827(11)	4.54699(14)
	0.4	0.798236(18)	1.728246(32)	2.544009(44)	3.316608(55)
	0.6	0.5691755(75)	1.283151(13)	1.886612(17)	2.447216(22)
	0.8	0.4362111(38)	1.0377647(63)	1.5383891(83)	1.989559(11)
5	0.194	1.431378(91)	3.03675(16)	4.49434(22)	5.86769(29)
	0.4	0.808461(20)	1.757499(36)	2.597493(51)	3.396810(65)
	0.6	0.5722526(77)	1.292481(13)	1.904940(19)	2.476827(24)
	0.8	0.4371741(39)	1.0407975(65)	1.5447616(86)	2.000643(11)
	0.9	0.3876830(29)	0.9510722(49)	1.4215906(63)	1.8418824(80)
6	0.138	1.91475(23)	4.06357(42)	6.02429(55)	7.86806(66)
	0.45	0.739093(19)	1.623965(33)	2.403967(45)	3.147423(57)
	0.55	0.621096(13)	1.389882(21)	2.052994(29)	2.679049(36)
	0.65	0.5342576(87)	1.222777(15)	1.806579(20)	2.349544(24)

TABLE VI. Quenched QED corrections, for quark electric charge $e/3$, to the time-moments given for a subset of the results in Table V for the $(n-2)$ th root of the unrenormalised G_n^V/Z_V^2 . The results are given as the ratio, R^0 , of the value in QCD+QED to that in pure QCD at fixed valence quark mass in lattice units.

Set	am_h	$n=4$	$n=6$	$n=8$	$n=10$
2	0.866	0.999669(32)	0.999731(16)	0.999697(11)	0.999641(8)
3	0.274	0.999774(30)	0.999692(25)	0.999646(24)	0.999622(24)
	0.548	0.999475(43)	0.999353(22)	0.999194(14)	0.999060(11)

current is not renormalised in these raw results and QED effects in Z_V must also be taken into account, as for the decay constant [14]. These results are also plotted in Fig. 8 as the cyan points. The impact of QED is not visible.

To fit the time-moment results as a function of lattice spacing and heavy quark mass we again use the fit of Eq. (4), supplemented with QED effects in Eq. (7). For the time-moments we use $F_0 = (c_F^{(0)} + c_F^{(1)}(3 \text{ GeV})/M_{\phi_h})$, and the dimensionful parameter A is taken as 0.5 GeV^{-1} for every moment. The prior values on $c_F^{(0)}$ and $c_F^{(1)}$ are taken to be 0 ± 1 for each moment. We fit all moments separately using an SVD cut of 5×10^{-4} in all cases. The χ^2/dof of the fits, in order of increasing n , are 0.9, 0.19, 0.26 and 0.4. The curves in Fig. 8 show the fit results evaluated at zero lattice spacing and with tuned sea quark masses.

Table VII gives our results for the time-moments evaluated at the b quark mass in the continuum limit, with

their total uncertainties. The corresponding error budget is given in Table VIII. In the next section we compare these results to earlier lattice analyses and values determined from experimental data for $R(e^+e^- \rightarrow \text{hadrons})$. We will also use the results to improve the determination of the b quark contribution to the hadronic vacuum polarisation term in the Standard Model determination of the anomalous magnetic moment of the muon. Column 3 of Table VII gives the ratio of the QCD+QED result to that in pure QCD for each moment. Again we are not able to distinguish any impact of QED on the results at the level of our uncertainties (which range from 0.4% down to 0.1%).

A. Discussion: time moments and a_μ^b

In Fig. 9 we compare our results for the time-moments to those of an earlier HPQCD calculation that used

TABLE VII. Results for the time moments of the bottomonium vector current-current correlator obtained from evaluating our fit functions in the continuum limit at the b quark mass. These are given in the second column for moment numbers listed in the first column. The results extracted from experimental data in [57] are given in the third column for comparison. The fourth column gives the quenched QED correction to these moments, as a ratio of the value in QCD plus QED to that in pure QCD with a tuned b quark mass (to reproduce the Υ mass from experiment) in both cases. All of the ratios are consistent with 1.0.

n	$G_n^{1/(n-2)}$ [GeV $^{-1}$]	$(G_n^{\text{exp.}})^{1/(n-2)}$ [GeV $^{-1}$]	$R_{\text{QED}} \left[G_n^{1/(n-2)} \right]$
4	0.0905(23)	0.09151(31)	0.9996(38)
6	0.1920(39)	0.19910(49)	0.9999(19)
8	0.2934(55)	0.29964(55)	0.9999(13)
10	0.3918(66)	0.39548(59)	0.9999(10)

TABLE VIII. Error budget for the n th time-moment, $G_n^{1/(n-2)}$, as a percentage of the final answer.

n	4	6	8	10
statistics	0.25	0.27	0.27	0.24
SVD cut	1.84	1.63	1.50	1.34
w_0	0.59	0.62	0.62	0.58
w_0/a	0.39	0.31	0.33	0.23
Z_V	0.13	0.04	0.02	0.01
F_0	0.01	0.02	0.02	0.03
G_0	0.01	0.01	0.01	0.02
G_1	0.75	0.35	0.26	0.28
G_2	0.42	0.31	0.24	0.42
G_3	0.43	0.14	0.14	0.19
G_4	0.57	0.36	0.32	0.31
G_5	0.97	0.71	0.67	0.42
\hat{G}_1	0.34	0.18	0.12	0.09
\hat{G}_2	0.01	0.00	0.00	0.00
Total (%)	2.54	2.03	1.87	1.68

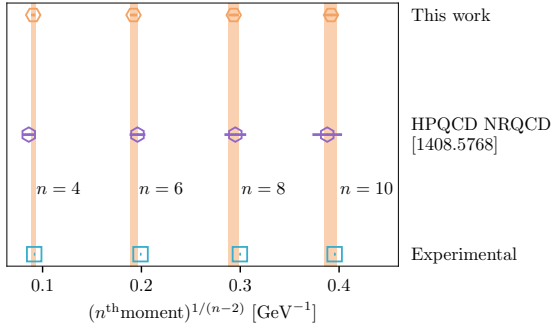


FIG. 9. Comparison of different determinations of the four lowest time moments of the bottomonium vector current-current correlator. The three determinations are, from the top, this work, previous calculation by the HPQCD collaboration using NRQCD b quarks [13] and the values obtained from experimental data on $R(e^+e^- \rightarrow \text{hadrons})$ in [57].

NRQCD b quarks [13]. For the NRQCD results the key sources of error were from the vector current normalisation (using a method based on matching the time-moments to continuum perturbation theory) and from the lattice spacing dependence effects in the NRQCD action. Our uncertainties here are a considerable improvement (by over a factor of two) on the NRQCD results, because we have a very accurate vector current normalisation and have results over a large range of lattice spacing values to control the lattice spacing dependence.

Figure 9 shows that our results agree within 2σ with the values extracted for the q^2 -derivative moments, \mathcal{M}_k ($n = 2k + 2$), of the b quark vacuum polarization using experimental values for $R_{e^+e^-} = \sigma(e^+e^- \rightarrow \text{hadrons})/\sigma_{pt}$ [57]. The appropriate normalisation of these results for the comparison to ours, is:

$$G_n^{\text{exp}} = \left(\frac{\mathcal{M}_k^{\text{exp}} n!}{12\pi^2 e_b^2} \right)^{1/(n-2)} \quad (26)$$

Our results from lattice QCD have considerably larger uncertainties than those of the experimental values but together these results provide a further test of QCD at the level of 2%.

We may also use these time-moments to extract the b quark connected contribution to the leading order hadronic vacuum polarisation contribution to the anomalous magnetic moment of the muon. This was done in [13] and, given that we have improved on the time-moments of that work, we provide an update here. We obtain

$$a_\mu^b = 0.300(15) \times 10^{-10} \quad (27)$$

This agrees with the value in [13] with an improvement in uncertainty of a factor of 2.5. Since the b quark is so heavy, this is not a significant contribution to the anomalous magnetic moment of the muon [58].

VI. CONCLUSIONS

We have used the fully relativistic HISQ action to calculate the masses and decay constants of ground-state bottomonium mesons in lattice QCD including the effects of u , d , s and c quarks in the sea. We have used very fine lattices and a range of heavy quark masses at each lattice spacing to control the discretisation effects as a function of heavy quark mass along with the physical dependence on the heavy quark mass of the quantities being studied. We have used a fit function with completely generic dependence on the heavy quark mass in each of its component pieces, capturing this dependence through cubic spline functions. Values for bottomonium are obtained by evaluating the fit function at zero lattice spacing with tuned sea quark masses and a valence quark mass tuned to that of the b , defined to be the point at which the Υ mass agrees with experiment. We have also included an analysis of the impact of the electric charge of the valence b quarks on the quantities being studied.

The results given are from the QCD+QED fit but, in all cases, we find the impact of QED to be negligible at the level of our uncertainties.

Our results yield the most precise, to date, lattice calculation of the bottomonium hyperfine splitting. We obtain the value (repeating Eq. (11)):

$$M_{\Upsilon} - M_{\eta_b} = 57.5(2.3)(1.0) \text{ MeV}. \quad (28)$$

The first uncertainty is from our fit results (see error budget in Table IV) and the second uncertainty is from an estimate of missing quark-line disconnected contributions that would affect the mass of the η_b meson. Our result is in agreement with, but on the low side of, the experimental average value [1]. It tends to favour the most recent experimental result obtained by the BELLE collaboration [32], although uncertainties (both ours and from the experiment) are still too large to draw strong conclusions from this.

We also provide the most precise lattice QCD determination of the Υ decay constant, which can be used to determine the Υ leptonic width. Our uncertainty of 1.5% is three times better than the previous lattice QCD calculation of [13]. The big advantage of using a relativistic formalism, as we do here, is that the vector current can be normalised very accurately and nonperturbatively [14]. Our result (repeating Eq. (16)) is

$$f_{\Upsilon} = 677.2(9.7) \text{ MeV}, \quad (29)$$

with error budget in Table IV. Using this result to obtain the Υ leptonic width gives (repeating Eq. (23)):

$$\Gamma(\Upsilon \rightarrow e^+e^-) = 1.292(37)(3) \text{ keV}. \quad (30)$$

The first uncertainty is from our result for f_{Υ} and the second from possible $\mathcal{O}(\alpha_{\text{QED}}/\pi)$ corrections to the formula connecting decay constant and leptonic width (Eq. (14)). This is to be compared with the current experimental average of 1.340(18) keV [1]. We see that our result is in good agreement with experiment and our uncertainty is just twice as large.

The decay constant of the η_b can also be accurately calculated with our approach. There is no experimental decay rate that can be directly compared to this determination, but the value of f_{η_b} is important for our phenomenological understanding of the relationships between decay constants for different mesons. We obtain (repeating Eq. (18))

$$f_{\eta_b} = 724(12) \text{ MeV}. \quad (31)$$

In particular, repeating Eq. (20), we find that

$$\frac{f_{\Upsilon}}{f_{\eta_b}} = 0.9454(99), \quad (32)$$

i.e. less than 1. This is in contrast to the charmonium case where $f_{J/\psi}/f_{\eta_c}$ is larger than 1 [9]. Fig. 5 shows how the ratio of the decay constants for vector and pseudoscalar heavyonium mesons varies with heavy quark

mass. This is qualitatively similar to the behaviour seen for the decay constants of heavy-light mesons [47]. Finally, in Fig. (7) we plot the ratios of mass to decay constant for pseudoscalar and vector mesons as a function of the ratio of pseudoscalar to vector meson masses. These may provide useful information to constrain these ratios in QCD-like beyond the Standard Model scenarios.

The low time moments of the bottomonium vector current-current correlator provide a further opportunity to compare lattice QCD results to experiment, where the matching inverse- s moments of the b -quark contribution to $R(e^+e^- \rightarrow \text{hadrons})$ can be determined. Our results for the 4th, 6th, 8th and 10th time moments are given in Table VII where they can be compared to the results obtained from experiment. Our uncertainties are 2% so provide the most accurate test to date for these quantities. The time moments can be used to determine the b quark contribution to the anomalous magnetic moment of the muon. We find (repeating Eq. (27))

$$a_{\mu}^b = 0.300(15) \times 10^{-10}. \quad (33)$$

Together these results demonstrate how the properties of low-lying bottomonium states can be determined in a fully relativistic calculation in lattice QCD and the gains in precision that such an approach makes possible. The results given here also allow us to improve the fully non-perturbative determination of the ratio of quark masses, m_b to m_c . We will present this analysis separately.

Acknowledgements

We are grateful to the MILC collaboration for the use of their gluon field configurations and for the use of MILC's QCD code. We have modified the code to generate quenched U(1) gauge fields and incorporate those into the quark propagator calculation as described here. We are grateful to B. Galloway for contributions to this project at a very early stage, and to R. Horgan, C. McNeile and J. Rosner for useful discussions. Computing was done on the Darwin supercomputer at the University of Cambridge High Performance Computing Service as part of the DiRAC facility, jointly funded by the Science and Technology Facilities Council, the Large Facilities Capital Fund of BIS and the Universities of Cambridge and Glasgow. We are grateful to the Darwin support staff for assistance. Funding for this work came from the Science and Technology Facilities Council and the National Science Foundation.

Appendix A: Reconstructing the heavy quark mass dependence

We give here the fit parameters that enable our fit results for the dependence on heavy quark mass of the hyperfine splitting, decay constants and ratio of decay constants to be reconstructed. The pieces of Eq. (4) that give

TABLE IX. Fit parameters for F_0 and G_0 for the fit of Eq. (4) to the hyperfine splitting as a function of the vector heavyonium mass, M_{ϕ_h} . The dimensionful constant, A is 0.1 GeV in this case and $F_0 = c_F^{(0)} + c_F^{(1)} \times 3 \text{ GeV}/M_{\phi_h}$. The mean and standard deviation for $c_F^{(0)}$ and $c_F^{(1)}$ and the values at the 3 knot positions for G_0 are: $c_F^{(0)} = 0.4407(6371)$; $c_F^{(1)} = 0.5031(7476)$; $G_0^{k1} = 0.3790(7089)$; $G_0^{k2} = 0.0956(5041)$; $G_0^{k3} = -0.0338(5285)$. The correlation matrix for these 5 parameters is given below. These results enable the red fit curve of Figure 1 to be reconstructed within the errors given.

$c_F^{(0)}$	$c_F^{(1)}$	G_0^{k1}	G_0^{k2}	G_0^{k3}
1.0	-0.6195	-0.1146	-0.7011	-0.9420
-0.6195	1.0	-0.7084	-0.1250	0.3225
-0.1146	-0.7084	1.0	0.7878	0.4386
-0.7011	-0.1250	0.7878	1.0	0.8980
-0.9420	0.3225	0.4386	0.8980	1.0

TABLE X. Fit parameters for F_0 and G_0 for the fit of Eq. (4) to the vector decay constant of the vector heavyonium ϕ_h meson (upper set) and the decay constant of the pseudoscalar heavyonium η_h meson (lower set), both as a function of the mass M_{ϕ_h} . The dimensionful constant, A is 0.7 GeV in these cases and $F_0 = c_F^{(0)} + c_F^{(1)} \times M_{\phi_h}/3 \text{ GeV}$. The top row of each set gives the mean and standard deviation for $c_F^{(0)}$ and $c_F^{(1)}$ and the values at the 3 knot positions for G_0 . The correlation matrix for these 5 parameters is given underneath. These results enable the red fit curves of both plots of Figure 4 to be reconstructed within the errors given.

f_{ϕ_h}				
$c_F^{(0)}$	$c_F^{(1)}$	G_0^{k1}	G_0^{k2}	G_0^{k3}
0.3487(3783)	0.1797(110)	0.030(378)	0.065(378)	0.051(378)
1.0	-0.0393	-0.9994	-0.9987	-0.9973
-0.0393	1.0	0.0279	-0.0080	-0.0289
-0.9994	0.0279	1.0	0.9986	0.9974
-0.9987	-0.0080	0.9986	1.0	0.9997
-0.9973	-0.0289	0.9974	0.9997	1.0
f_{η_h}				
$c_F^{(0)}$	$c_F^{(1)}$	G_0^{k1}	G_0^{k2}	G_0^{k3}
0.3487(3783)	0.1797(110)	0.005(378)	0.077(378)	0.122(378)
1.0	-0.0399	-0.9993	-0.9987	-0.9962
-0.0393	1.0	0.0146	-0.0076	-0.0372
-0.9993	0.0146	1.0	0.9992	0.9977
-0.9987	-0.0076	0.9992	1.0	0.9992
-0.9962	-0.0372	0.9977	0.9992	1.0

the physical curves in the continuum limit are $F_0(M_{\phi_h})$ and $G_0(1/M_{\phi_h})$, multiplied by dimensionful constant, A (absent for the case of the ratio of decay constants). We ignore here the QED pieces of the fit; these have negligible effect in all cases.

F_0 is a simple function with at most two parameters, $c_F^{(0)}$ and $c_F^{(1)}$. G_0 is a Steffen spline function [23] with 3 knots at 2.5, 4.9 and 10.0 GeV in M_{ϕ_h} , so that in $1/M_{\phi_h}$ they are at $1/2.5$, $1/4.9$ and $1/10.0$. Tables IX, X and XI give the mean and standard deviation of $c_F^{(0)}$, $c_F^{(1)}$, and the values at the 3 knots of G_0 : G_0^{k1} , G_0^{k2} and G_0^{k3} . This is followed underneath by the correlation matrix between these parameters. The parameters are strongly correlated and this is why we give the values to 4 significant figures. The splines can easily be implemented using the `gvar` Python module [26].

TABLE XI. Fit parameters for F_0 and G_0 for the fit of Eq. (4) to the ratio of vector to pseudoscalar heavyonium decay constants as a function of the mass of the vector heavyonium meson, M_{ϕ_h} . F_0 is simply a constant, $c_F^{(0)}$ in this case. The top row gives the mean and standard deviation for $c_F^{(0)}$ and the values at the 3 knot positions for G_0 . The correlation matrix for these 4 parameters is given underneath. These results enable the red fit curve of Figure 5 to be reconstructed within the errors given.

$c_F^{(0)}$	G_0^{k1}	G_0^{k2}	G_0^{k3}
0.9973(2080)	0.0691(2081)	-0.0169(2080)	-0.0538(2082)
1.0	-0.9992	-0.9998	-0.9988
-0.9992	1.0	0.9991	0.9983
-0.9998	0.9991	1.0	0.9993
-0.9988	0.9983	0.9993	1.0

-
- [1] P. Zyla *et al.* (Particle Data Group), *PTEP* **2020**, 083C01 (2020).
 - [2] E. McLean, C. Davies, J. Koponen, and A. Lytle, *Phys. Rev. D* **101**, 074513 (2020), [arXiv:1906.00701 \[hep-lat\]](#).
 - [3] J. Harrison, C. T. H. Davies, and A. Lytle (HPQCD), *Phys. Rev. D* **102**, 094518 (2020), [arXiv:2007.06957 \[hep-lat\]](#).
 - [4] E. Follana *et al.* (HPQCD Collaboration), *Phys. Rev. D* **75**, 054502 (2007), [arXiv:hep-lat/0610092 \[hep-lat\]](#).
 - [5] E. Follana, C. Davies, G. Lepage, and J. Shigemitsu (HPQCD Collaboration), *Phys. Rev. Lett.* **100**, 062002 (2008), [arXiv:0706.1726 \[hep-lat\]](#).
 - [6] C. Davies, C. McNeile, E. Follana, G. Lepage, H. Na, *et al.* (HPQCD Collaboration), *Phys. Rev. D* **82**, 114504 (2010), [arXiv:1008.4018 \[hep-lat\]](#).
 - [7] H. Na, C. T. Davies, E. Follana, G. P. Lepage, and J. Shigemitsu (HPQCD Collaboration), *Phys. Rev. D* **82**, 114506 (2010), [arXiv:1008.4562 \[hep-lat\]](#).
 - [8] G. Donald, C. Davies, R. Dowdall, E. Follana, K. Hornbostel, *et al.* (HPQCD collaboration), *Phys. Rev. D* **86**, 094501 (2012), [arXiv:1208.2855 \[hep-lat\]](#).
 - [9] D. Hatton, C. Davies, B. Galloway, J. Koponen, G. Lepage, and A. Lytle (HPQCD), *Phys. Rev. D* **102**, 054511 (2020), [arXiv:2005.01845 \[hep-lat\]](#).
 - [10] C. McNeile, C. Davies, E. Follana, K. Hornbostel, and G. Lepage (HPQCD Collaboration), *Phys. Rev. D* **85**, 031503 (2012), [arXiv:1110.4510 \[hep-lat\]](#).
 - [11] C. McNeile, C. Davies, E. Follana, K. Hornbostel, and G. Lepage, *Phys. Rev. D* **86**, 074503 (2012), [arXiv:1207.0994 \[hep-lat\]](#).
 - [12] A. Bazavov *et al.*, *Phys. Rev. D* **98**, 074512 (2018), [arXiv:1712.09262 \[hep-lat\]](#).
 - [13] B. Colquhoun, R. Dowdall, C. Davies, K. Hornbostel, and G. Lepage, *Phys. Rev. D* **91**, 074514 (2015), [arXiv:1408.5768 \[hep-lat\]](#).
 - [14] D. Hatton, C. Davies, G. Lepage, and A. Lytle (HPQCD), *Phys. Rev. D* **100**, 114513 (2019), [arXiv:1909.00756 \[hep-lat\]](#).
 - [15] A. Bazavov *et al.* (MILC), *Phys. Rev. D* **87**, 054505 (2013), [arXiv:1212.4768 \[hep-lat\]](#).
 - [16] A. Hart, G. M. von Hippel, and R. R. Horgan (HPQCD), *Phys. Rev. D* **79**, 074008 (2009), [arXiv:0812.0503 \[hep-lat\]](#).
 - [17] S. Borsanyi, S. Durr, Z. Fodor, C. Hoelbling, S. D. Katz, *et al.*, *JHEP* **1209**, 010 (2012), [arXiv:1203.4469 \[hep-lat\]](#).
 - [18] C. Bernard and D. Toussaint (MILC), *Phys. Rev. D* **97**, 074502 (2018), [arXiv:1707.05430 \[hep-lat\]](#).
 - [19] R. Dowdall, C. Davies, G. Lepage, and C. McNeile (HPQCD), *Phys. Rev. D* **88**, 074504 (2013), [arXiv:1303.1670 \[hep-lat\]](#).
 - [20] D. Hatton, C. Davies, and G. Lepage, *Phys. Rev. D* **102**, 094514 (2020), [arXiv:2009.07667 \[hep-lat\]](#).
 - [21] G. P. Lepage *et al.*, *Nucl. Phys. Proc. Suppl.* **106**, 12 (2002), [arXiv:hep-lat/0110175](#).
 - [22] M. Hayakawa and S. Uno, *Prog. Theor. Phys.* **120**, 413 (2008), [arXiv:0804.2044 \[hep-ph\]](#).
 - [23] M. Steffen, *Astron. Astrophys.* **239**, 443 (1990).
 - [24] R. Dowdall, C. Davies, R. Horgan, G. Lepage, C. Monahan, J. Shigemitsu, and M. Wingate, *Phys. Rev. D* **100**, 094508 (2019), [arXiv:1907.01025 \[hep-lat\]](#).
 - [25] G. P. Lepage, *lsqfit* v. 11.7, <https://github.com/gplepage/lsqfit>, doi:10.5281/zenodo.4037174 (2020).
 - [26] G. P. Lepage, *gvar* v. 11.9.1, <https://github.com/gplepage/gvar>, doi:10.5281/zenodo.4290884 (2020).
 - [27] A. Gray, I. Allison, C. Davies, E. Dalgic, G. Lepage, *et al.* (HPQCD Collaboration), *Phys. Rev. D* **72**, 094507 (2005), [arXiv:hep-lat/0507013 \[hep-lat\]](#).
 - [28] T. Burch, C. DeTar, M. Di Pierro, A. X. El-Khadra, E. D. Freeland, S. Gottlieb, A. S. Kronfeld, L. Levkova, P. B. Mackenzie, and J. N. Simone, *Phys. Rev. D* **81**, 034508 (2010), [arXiv:0912.2701 \[hep-lat\]](#).
 - [29] S. Meinel, *Phys. Rev. D* **82**, 114502 (2010), [arXiv:1007.3966 \[hep-lat\]](#).
 - [30] Y. Aoki, N. H. Christ, J. M. Flynn, T. Izubuchi, C. Lehner, M. Li, H. Peng, A. Soni, R. S. Van de Water, and O. Witzel (RBC, UKQCD), *Phys. Rev. D* **86**, 116003 (2012), [arXiv:1206.2554 \[hep-lat\]](#).
 - [31] R. J. Dowdall, C. T. H. Davies, T. Hammant, R. R. Horgan, and C. Hughes (HPQCD), *Phys. Rev. D* **89**, 031502 (2014), [Erratum: *Phys. Rev. D* **92**, 039904 (2015)], [arXiv:1309.5797 \[hep-lat\]](#).
 - [32] R. Mizuk *et al.* (Belle), *Phys. Rev. Lett.* **109**, 232002 (2012), [arXiv:1205.6351 \[hep-ex\]](#).
 - [33] G. Bonvicini *et al.* (CLEO), *Phys. Rev. D* **81**, 031104 (2010), [arXiv:0909.5474 \[hep-ex\]](#).
 - [34] B. Aubert *et al.* (BaBar), *Phys. Rev. Lett.* **103**, 161801 (2009), [arXiv:0903.1124 \[hep-ex\]](#).
 - [35] B. Aubert *et al.* (BaBar), *Phys. Rev. Lett.* **101**, 071801 (2008), [Erratum: *Phys. Rev. Lett.* **102**, 029901 (2009)], [arXiv:0807.1086 \[hep-ex\]](#).
 - [36] A. X. El-Khadra, A. S. Kronfeld, and P. B. Mackenzie, *Phys. Rev. D* **55**, 3933 (1997), [arXiv:hep-lat/9604004 \[hep-lat\]](#).
 - [37] L. Levkova and C. DeTar, *Phys. Rev. D* **83**, 074504 (2011), [arXiv:1012.1837 \[hep-lat\]](#).
 - [38] S. M. Ryan and D. J. Wilson (Hadron Spectrum), (2020), [arXiv:2008.02656 \[hep-lat\]](#).
 - [39] Y. Aoki *et al.*, *Phys. Rev. D* **78**, 054510 (2008), [arXiv:0712.1061 \[hep-lat\]](#).
 - [40] C. Sturm, Y. Aoki, N. Christ, T. Izubuchi, C. Sachrajda, and A. Soni, *Phys. Rev. D* **80**, 014501 (2009), [arXiv:0901.2599 \[hep-ph\]](#).
 - [41] A. Pivovarov, *Phys. Atom. Nucl.* **65**, 1319 (2002), [arXiv:hep-ph/0011135](#).
 - [42] C. Davies, *Lect. Notes Phys.* **512**, 1 (1998), [arXiv:hep-ph/9710394](#).
 - [43] B. Jones and R. Woloshyn, *Phys. Rev. D* **60**, 014502 (1999), [arXiv:hep-lat/9812008](#).
 - [44] G. Donald, C. Davies, J. Koponen, and G. Lepage, *Phys. Rev. Lett.* **112**, 212002 (2014), [arXiv:1312.5264 \[hep-lat\]](#).
 - [45] V. Lubicz, A. Melis, and S. Simula (ETM), *Phys. Rev. D* **96**, 034524 (2017), [arXiv:1707.04529 \[hep-lat\]](#).
 - [46] Y. Chen, W.-F. Chiu, M. Gong, Z. Liu, and Y. Ma (chiQCD), (2020), [arXiv:2008.05208 \[hep-lat\]](#).
 - [47] B. Colquhoun, C. Davies, R. Dowdall, J. Kettle, J. Koponen, G. Lepage, and A. Lytle (HPQCD), *Phys. Rev. D* **91**, 114509 (2015), [arXiv:1503.05762 \[hep-lat\]](#).
 - [48] S. Bekavac, A. Grozin, P. Marquard, J. Piclum, D. Seidel, and M. Steinhauser, *Nucl. Phys. B* **833**, 46 (2010), [arXiv:0911.3356 \[hep-ph\]](#).

- [49] T. DeGrand and E. T. Neil, *Phys. Rev. D* **101**, 034504 (2020), [arXiv:1910.08561 \[hep-ph\]](#).
- [50] W. Kwong, J. L. Rosner, and C. Quigg, *Ann.Rev.Nucl.Part.Sci.* **37**, 325 (1987).
- [51] E. J. Eichten and C. Quigg, *Phys.Rev.* **D52**, 1726 (1995), [arXiv:hep-ph/9503356 \[hep-ph\]](#).
- [52] E. Eichten, S. Godfrey, H. Mahlke, and J. L. Rosner, *Rev.Mod.Phys.* **80**, 1161 (2008), [arXiv:hep-ph/0701208 \[hep-ph\]](#).
- [53] Y. Hochberg, E. Kuflik, H. Murayama, T. Volansky, and J. G. Wacker, *Phys. Rev. Lett.* **115**, 021301 (2015), [arXiv:1411.3727 \[hep-ph\]](#).
- [54] K. Harigaya and Y. Nomura, *Phys. Rev. D* **94**, 035013 (2016), [arXiv:1603.03430 \[hep-ph\]](#).
- [55] B. Chakraborty, C. Davies, G. Donald, J. Koponen, and G. Lepage (HPQCD), *Phys. Rev. D* **96**, 074502 (2017), [arXiv:1703.05552 \[hep-lat\]](#).
- [56] I. Allison *et al.*, *Phys.Rev.* **D78**, 054513 (2008), [arXiv:0805.2999 \[hep-lat\]](#).
- [57] J. H. Kuhn, M. Steinhauser, and C. Sturm, *Nucl.Phys.* **B778**, 192 (2007), [arXiv:hep-ph/0702103 \[HEP-PH\]](#).
- [58] T. Aoyama *et al.*, *Phys. Rept.* **887**, 1 (2020), [arXiv:2006.04822 \[hep-ph\]](#).